Precision Engineering 50 (2017) 235–247

Contents lists available at ScienceDirect

Precision Engineering

journal homepage: www.elsevier.com/locate/precision

Robust weighting applied to optimization of AISI H13 hardened-steel turning process with ceramic wiper tool: A diversity-based approach

Luiz Célio Souza Rocha[a,b], Anderson Paulo de Paiva[b], Paulo Rotela Junior[c,*], Pedro Paulo Balestrassi[b], Paulo Henrique da Silva Campos[b], João Paulo Davim[d]

[a] Federal Institute of Education, Science and Technology – South of Minas Gerais, Machado, MG, Brazil
[b] Institute of Production Engineering and Management, Federal University of Itajubá, Itajubá, MG, Brazil
[c] Production Engineering Department, Federal University of Paraíba, João Pessoa, PB, Brazil
[d] Department of Mechanical Engineering, University of Aveiro, Aveiro, Portugal

ARTICLE INFO

Article history:
Received 12 January 2017
Received in revised form 29 April 2017
Accepted 16 May 2017
Available online 19 May 2017

Keywords:
Wiper ceramic tool
Hard turning
Robust weighting
Diversity
Normal boundary intersection
Mixture design of experiments
Multiobjective optimization

ABSTRACT

A mixed ceramic is a type of cutting-tool material widely employed for machining hardened steels. The usage of a mixed ceramic along with a wiper geometry can help double the feed rate, thereby increasing productivity while keeping the surface roughness (*Ra*) as low as possible. Analyses of manufacturing processes, such as a machining process, show that the various possible controlled parameters can be modeled by multiobjective mathematical models to ensure their optimization. Hence, the aim of this study was optimize a hard turning process using a robust weighting based on diversity to choose the final Pareto optimal solution of the multiobjective problem. The responses of the material removal rate (*MRR*), *Ra* parameter, and cutting force (*Fc*) were modeled by using the response surface methodology; in this methodology, decision variables, such as the cutting speed (*Vc*), feed rate (*f*), and depth of cut (*d*), are employed. The diversity index, as a decision-making criterion, proved to be useful in mapping the regions of minimum variance within the Pareto optimal responses obtained in the optimization process. Hence, the study demonstrates that the weights used in the multiobjective optimization process influence the prediction variance of the obtained response.

1. Introduction

Precision turning of hardened steel is a highly flexible, productive, and cost effective machining process for machining ferrous metal components, which are usually hardened over 45 HRC [1–3]. Hardened steels are widely employed in various fields of engineering owing to their high hardness, high strength, and good wear resistance [4]. The turning operation is performed using materials required for advanced tools, yielding significant benefits, such as a low surface roughness (*Ra*), high material removal rate (*MRR*), and short cutting time cycle [3,5]. As a result, hard turning is replacing grinding in many industrial applications [1,3,6,7].

Many types of cutting tools are used for turning hardened steels. A mixed ceramic (aluminum oxide along with TiC or TiN) is a type of cutting-tool material widely employed for machining hardened steels [8,9], particularly under dry cutting conditions and moderate cutting speeds ranging between 90 and 120 m/min [9]. The ceramic cutting tools are used to machine superhard materials, which are difficult to machine using conventional tool materials [10].

Furthermore, the optimum cutting speed employed while using the ceramic cutting tools is three to ten times higher than that employed when using normal cemented carbide tools with the same geometrical parameters; hence, the processing efficiency is higher [10]. Several scholars have conducted extensive studies on the development of ceramic cutting tools [10–16].

Some researchers who studied the influence of tool geometry proposed the use of tools having wiper geometry in order to improve the hard turning process [1,7,8,12,17]. Owing to their three radii geometries [1], such tools can double the feed rate, thereby increasing productivity while keeping the *Ra* as low as possible [1,7,17]. Fig. 1 shows the conventional and wiper (multi-radii) geometries.

* Corresponding author at: Production Engineering Department, Federal University of Paraíba, Cidade Universitária, s/n, João Pessoa, PB 58051-900, Brazil.
E-mail addresses: luizrochamg@hotmail.com (L.C.S. Rocha), andersonppaiva@unifei.edu.br (A.P. de Paiva), paulo.rotela@gmail.com (P. Rotela Junior), ppbalestrassi@gmail.com (P.P. Balestrassi), paulohcamposs@hotmail.com (P.H. da Silva Campos), pdavim@ua.pt (J.P. Davim).

http://dx.doi.org/10.1016/j.precisioneng.2017.05.011
0141-6359/

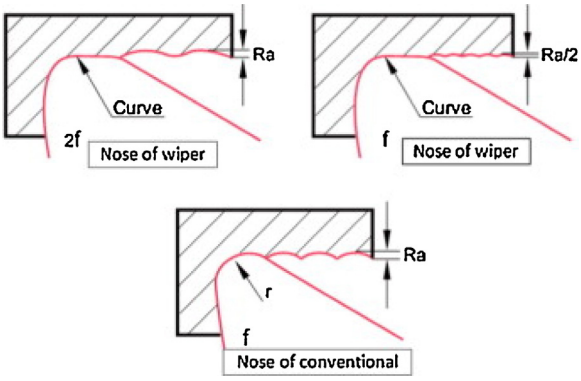

Fig. 1. Surface generation using wiper and conventional inserts [18].

The potential benefits of hard turning, such as an improvement in the surface quality and productivity rate, depend intrinsically on an optimal setup of the process parameters, such as the cutting speed (*Vc*), feed rate (*f*), and depth of cut (*d*). These parameters are directly responsible for many of the machining's predictable properties, such as the tool wear, tool life, surface finishing, and amount of material removed [1,7,11,17].

Analyses of manufacturing processes, such as the machining process, show that the various possible controlled parameters lead to multiobjective mathematical models that can be used to ensure the process' optimization. When working with multiobjective optimization, besides searching for the point that characterizes the final solution of the problem, the reliability of the obtained solution is a major factor that needs to be considered. Hence, the forecast variance is a major concern [19]. To the best of our knowledge, the ways in which the weighting in the multiobjective optimization affects the prediction variance, for a particular experimental design, have never been studied; hence, it provides a scope for exploring the theoretical contributions pertaining to this topic.

Therefore, the main objective of this study was to optimize the turning process of AISI H13 hardened steel with a ceramic wiper tool using a robust weighting based on diversity [20] to choose the most preferred Pareto optimal point as the final solution of the problem. The responses of the *MRR*, *Ra*, and cutting force (*Fc*) were modeled using the response surface methodology (RSM). The normal boundary intersection (NBI) method, along with the mixture design of experiments (MDE), were used to optimize these responses simultaneously. The decision variables were the *Vc*, *f*, and *d*.

2. Design of experiments

According to Montgomery [21], an experiment can be defined as a series of tests wherein required changes are made to the input variables of a process in order to observe the effect of such changes on the responses. The design of experiments (DOE) is then defined as the process of planning the experiments so that the appropriate data is collected and then analyzed using statistical methods, thereby arriving at valid and objective conclusions.

In this study, the RSM and MDE, two widely used techniques, were utilized. The RSM is a collection of mathematical and statistical tools used to model and analyze problems wherein the responses of interest are influenced by several variables. The objective of the RSM is to optimize these responses [21,22]. For most industrial processes, the relationships between the responses and independent variables are unknown; hence, the RSM seeks to determine a suitable approximation to represent the responses of interest as a function of these variables. To describe such relationships, researchers generally use polynomial functions. Thus, if a response is well modeled by a quadratic function, the approximate ratio can be represented by the following second-order model:

$$y(x) = \beta_0 + \sum_{i=1}^{k}\beta_i x_i + \sum_{i=1}^{k}\beta_{ii}x_i^2 + \sum_{i<j}\sum\beta_{ij}x_i x_j + \varepsilon \tag{1}$$

where $y(x)$ is the response of interest; x_i and x_j are the independent variables; β_0 is the intercept coefficient to be estimated; β_i represents the linear coefficients to be estimated; β_{ii} represents the squared coefficients to be estimated; k is the number of independent variables; and ε is the experimental error.

Although it is unlikely that a polynomial model is the most ideal approach for the entire experimental space covered by the independent variables, such models have been shown to be effective for a specific region [21,22].

The estimation of the coefficients, defined by Eq. (1), is typically made using the ordinary least squares (OLS) method. The OLS method is based on choosing the values for β_i such that the sum of the squared errors is minimized. The OLS function can be written as [21,22]:

$$L = \sum_{i=1}^{k}\varepsilon_i^2 = \sum_{i=1}^{k}\left(y_i - \beta_0 - \sum_{i=1}^{k}\beta_i x_i\right)^2 \tag{2}$$

where y_i is the response of interest; x_i represents the independent variables; β_0 is the intercept coefficient to be estimated; β_i represents the coefficients to be estimated; k is the number of independent variable; and ε_i is the experimental error.

The response of interest may be written in matrix notation as

$$\mathbf{y} = \mathbf{X\beta} + \boldsymbol{\varepsilon} \tag{3}$$

where

$$\mathbf{y} = \begin{bmatrix} y_1 \\ y_2 \\ \vdots \\ y_n \end{bmatrix}, \quad \mathbf{X} = \begin{bmatrix} 1 & x_{11} & x_{12} & \cdots & x_{1k} \\ 1 & x_{21} & x_{22} & \cdots & x_{2k} \\ \vdots & \vdots & \vdots & \ddots & \vdots \\ 1 & x_{n1} & x_{n2} & \cdots & x_{nk} \end{bmatrix},$$

$$\boldsymbol{\beta} = \begin{bmatrix} \beta_0 \\ \beta_1 \\ \vdots \\ \beta_k \end{bmatrix}, \quad \boldsymbol{\varepsilon} = \begin{bmatrix} \varepsilon_1 \\ \varepsilon_2 \\ \vdots \\ \varepsilon_n \end{bmatrix} \tag{4}$$

Hence, L can be expressed as

$$L = \mathbf{y}^T\mathbf{y} - \boldsymbol{\beta}^T\mathbf{X}^T\mathbf{y} - \mathbf{y}^T\mathbf{X\beta} + \boldsymbol{\beta}^T\mathbf{X}^T\mathbf{X\beta} = \mathbf{y}^T\mathbf{y} - 2\boldsymbol{\beta}^T\mathbf{X}^T\mathbf{y} + \boldsymbol{\beta}^T\mathbf{X}^T\mathbf{X\beta} \tag{5}$$

As $\boldsymbol{\beta}^T\mathbf{X}^T\mathbf{y}$ is a 1×1 matrix, or a scalar, and its transpose $(\boldsymbol{\beta}^T\mathbf{X}^T\mathbf{y})^T = \mathbf{y}^T\mathbf{X\beta}$ is the same scalar, the least squares estimators must satisfy

$$\frac{\partial L}{\partial \boldsymbol{\beta}} = -2\mathbf{X}^T\mathbf{y} + 2\mathbf{X}^T\mathbf{X}\beta = 0 \tag{6}$$

which simplifies to

$$\mathbf{X}^T\mathbf{X}\beta = \mathbf{X}^T\mathbf{y} \tag{7}$$

Eq. (7) expresses the set of normal equations for the least squares in matrix form. By multiplying both sides of Eq. (7) by the inverse of $\mathbf{X}^T\mathbf{X}$, the following is obtained:

$$\hat{\boldsymbol{\beta}} = \left(\mathbf{X}^T\mathbf{X}\right)^{-1}\mathbf{X}^T\mathbf{y} \tag{8}$$

where $\hat{\boldsymbol{\beta}}$ is the least square estimator vector, and $\mathbf{X}$ and $\mathbf{y}$ are represented in Eq. (4).

As the least square estimator $\hat{\boldsymbol{\beta}}$ is a linear combination of the observations, it is normally distributed with the mean vector $\boldsymbol{\beta}$ and covariance matrix $\sigma^2\left(\mathbf{X}^T\mathbf{X}\right)^{-1}$. Then, the statistic

$$\frac{\hat{\beta}_j - \beta_j}{\sqrt{\hat{\sigma}^2 C_{jj}}}, \quad j = 0, 1, \ldots, k \tag{9}$$

is distributed as t with $n-p$ degrees of freedom, where n is the number of experiments, p is the number of terms plus one (related to the intercept), C_{jj} is the jjth element of the matrix $\left(\mathbf{X}^T\mathbf{X}\right)^{-1}$, and $\hat{\sigma}^2$ is the estimate of the error variance obtained from equation

$$\hat{\sigma}^2 = \frac{SS_E}{n-p} \tag{10}$$

where SS_E is the residual (or error) sum of squares and is given by

$$SS_E = \mathbf{y}^T\mathbf{y} - \hat{\boldsymbol{\beta}}^T\mathbf{X}^T\mathbf{y} \tag{11}$$

Hence, since α is a significance level, a confidence interval of $100(1-\alpha)\%$ for the regression coefficient β_j, $j = 0, 1, \ldots, k$, is given by

$$\hat{\beta}_j - t_{\alpha/2,n-p}\sqrt{\hat{\sigma}^2 C_{jj}} \le \beta_j \le \hat{\beta}_j + t_{\alpha/2,n-p}\sqrt{\hat{\sigma}^2 C_{jj}} \tag{12}$$

Note that this confidence interval can be written as a function of the standard error of the regression coefficient $se(\hat{\beta}_j)$:

$$\hat{\beta}_j - t_{\alpha/2,n-p}se(\hat{\beta}_j) \le \beta_j \le \hat{\beta}_j + t_{\alpha/2,n-p}se(\hat{\beta}_j) \tag{13}$$

because $se(\hat{\beta}_j) = \sqrt{\hat{\sigma}^2 C_{jj}}$.

The confidence interval of the mean response can also be obtained at a particular point $\mathbf{X}_0^T = \begin{bmatrix} 1 & x_{01} & x_{02} & \cdots & x_{0k} \end{bmatrix}$. The mean response and estimated mean response at this point are given by $\mu_{y|\mathbf{x}_0} = \mathbf{X}_0^T\boldsymbol{\beta}$ and $\hat{y}(\mathbf{X}_0) = \mathbf{X}_0^T\hat{\boldsymbol{\beta}}$, respectively. This estimator is unbiased because $E[\hat{y}(\mathbf{X}_0)] = E(\mathbf{X}_0^T\hat{\boldsymbol{\beta}}) = \mathbf{X}_0^T\boldsymbol{\beta} = \mu_{y|\mathbf{x}_0}$, where $E[\,]$ and $E(\,)$ are the expected values of the presented terms.

The variance of $\hat{y}(\mathbf{X}_0)$ is:

$$\mathrm{Var}[\hat{y}(\mathbf{X}_0)] = \hat{\sigma}^2\mathbf{X}_0^T(\mathbf{X}^T\mathbf{X})^{-1}\mathbf{X}_0 \tag{14}$$

Hence, a confidence interval of $100(1-\alpha)\%$ for the mean response at the point $\mathbf{X}_0^T = \begin{bmatrix} 1 & x_{01} & x_{02} & \cdots & x_{0k} \end{bmatrix}$ is:

$$\hat{y}(\mathbf{X}_0) - t_{\alpha/2,n-p}\sqrt{\hat{\sigma}^2\mathbf{X}_0^T(\mathbf{X}^T\mathbf{X})^{-1}\mathbf{X}_0} \le \mu_{y|\mathbf{x}_0} \le \hat{y}(\mathbf{X}_0) + t_{\alpha/2,n-p}\sqrt{\hat{\sigma}^2\mathbf{X}_0^T(\mathbf{X}^T\mathbf{X})^{-1}\mathbf{X}_0} \tag{15}$$

Once the model is constructed, its statistical significance should be verified through an analysis of variance (ANOVA). The ANOVA, besides revealing the significance of the model as a whole, permits us to check whether the terms of the model are significant and whether they can be neglected.

The fit is represented by the coefficient of multiple determination (R^2), which represents the percentage of the observed data in the response that can be explained by the mathematical model. R^2 is defined as

$$R^2 = \frac{SS_R}{SS_T} = 1 - \frac{SS_E}{SS_T} \tag{16}$$

where SS_R is the regression sum of squares; SS_E is the residual (or error) sum of squares, as expressed in Eq. (11); and SS_T is the total sum of squares.

The regression sum of squares (SS_R) may be expressed as

$$SS_R = \hat{\boldsymbol{\beta}}^T\mathbf{X}^T\mathbf{y} - \frac{\left(\sum_{i=1}^n y_i\right)^2}{n} \tag{17}$$

and the total sum of squares (SS_T) is

$$SS_T = \mathbf{y}^T\mathbf{y} - \frac{\left(\sum_{i=1}^n y_i\right)^2}{n} \tag{18}$$

A more accurate parameter, an adjusted R^2, can be defined; it is given as

$$R^2_{adj} = 1 - \frac{n-1}{n-p}(1-R^2) \tag{19}$$

where n is the number of experiments; p is the number of terms plus one (related to the intercept).

For the modeling of the response surface functions, the experimental arrangement most often used for the data collection is the central composite design (CCD) [21]. The CCD, for k factors, is a matrix formed by three distinct groups of experimental elements: a full factorial 2^k or fractional 2^{k-p}, where p is the desired fraction of the experiment; a set of central points (cp); and a group of extreme levels called axial points, given by $2k$. The number of experiments required is given by the sum $2^{k\ or\ (k-p)} + cp + 2k$. In the CCD, the axial points are within a distance α of the central points, where $\alpha = (2^k)^{1/4}$ [23].

In the MDE, the factors are the ingredients of a mixture, and their levels are not independent. As the constraint $\sum_{i=1}^n x_i = 1$ exists, the polynomials employed in the mixture model are different from those utilized in the RSM. For example, the special cubic form is given by [21,24]

$$y = \sum_{i=1}^{q}\beta_i x_i + \sum\sum_{i<j}^{q}\beta_{ij}x_i x_j + \sum\sum\sum_{i<j<k}^{q}\beta_{ijk}x_i x_j x_k \tag{20}$$

where y is the response of interest; x_i, x_j, and x_k are the independent variables; β_i represents the linear coefficients to be estimated; β_{ij} represents the quadratic coefficients to be estimated; β_{ijk} represents the cubic coefficients to be estimated; and q is the number of ingredients in the mixture.

According to Cornell [24] and Anderson-Cook et al. [19], owing to their different shapes, the functions mentioned above are called Scheffé's polynomials or canonical polynomials of the mixtures. The coefficients are estimated in a way that is similar to the one used in the RSM, as are the statistical analyses.

The experimental arrangement most often used in the MDE is the simplex arrangement [24]. In this arrangement, the k input variables define the points whose proportions are assumed to consider $m+1$ equally spaced values between 0 and 1, where m is the lattice degree of the arrangement. The total number of experiments (N) is given by

$$N = \frac{(k+m-1)!}{m!(k-1)!} \tag{21}$$

Similar to the simplex arrangement, few of the points on the internal part are tested; it is important to include the central and axial points in the experimental design. The axial points could be defined as the permutations of all the terms $((m+1)/2m, 1/2m, \ldots, 1/2m)$.

3. Multiobjective optimization

The optimization problems involving industrial processes are often multiobjective, as they involve more than one desirable feature. If there is no conflict between the objective functions, a solution can be found, wherein each objective function attains its optimum value. In this case, no special method is required [25].

However, often these objectives are functions of the same set of decision variables and are in conflict [26]. To study the tradeoffs between these conflicting objectives and explore the options available, a multiobjective optimization problem (MOP) should be formulated. A general formulation is expressed as

$$\underset{x \in \Omega}{Min} \quad \Lambda = \left\{F_1(x), F_2(x), \ldots, F_k(x)\right\} \tag{22}$$

where Λ is the vector of the objective functions F_i for the k criteria, which are mutually conflicting. The vector of the decision variables x must belong to the feasible set Ω, which usually includes the problem constraints in the inequalities or equalities form

$$\Omega = \{x \in \mathbb{R}^n | g_r(x) \leq 0, \quad r \in I, \quad h_q(x) = 0, \quad q \in J\} \tag{23}$$

Here, g_r and h_q are the inequality and equality constraint functions, respectively; I and J are the index sets containing as many elements as there are inequality and equality constraints, respectively.

The multiobjective optimization methods attempt to produce a set of tradeoff solutions called Pareto optimal solutions, wherein the decision maker can choose a particular solution. A solution is called the Pareto optimal if no objective can be improved without sacrificing the other. The methods that allow the user to obtain the full set of Pareto optimal solutions should have priority, as they give the decision-maker the ability to select the best solution among those considered efficient.

According to Shahraki and Noorossana [27], two approaches can be used to solving problems with more than one objective function. One is based on optimizing an objective considering other objectives as constraints. In this approach, the most important considered objective function is prioritized, giving rise to the term prioritization. The other is based on converting all the objective functions into a single problem by reducing it to a scalar optimization problem; hence, the term scalarization is used. Scalarization refers to the conversion of the problem by aggregation of the components of the objective functions into a single or a family of single objective optimization problems with a real-valued objective function [25,28]. Many methods can be used for this purpose, among which are the weighted sum method and the NBI approach.

3.1. Weighted sum method

The weighted sum method is one of the most commonly used techniques for solving the MOP. According to Zhang and Yang [29], this is because of its relative simplicity and physical interpretation of the processes being analyzed.

This method is characterized as a sequence of problems, wherein the objective functions are converted into a scalar optimization problem by minimizing the objective convex combination of the different objectives, i.e., the global objective function is defined by a linear combination of the original objective function and its respective degrees of importance, as represented by the weights. In other words, among n weights, w_i are chosen such that $w_i \geq 0$, $i = 1, \ldots, n$ and $\sum_{i=1}^{n} w_i = 1$. The following problem is then solved:

$$\begin{aligned} \underset{x}{Min} \quad & \sum_{i=1}^{n} w_i f_i(x) = w^T F(x) \\ s.t.: \quad & h_q(x) = 0, \quad q = 1, 2, \ldots, l \\ & g_r(x) \leq 0, \quad r = 1, 2, \ldots, m \end{aligned} \tag{24}$$

where $f_i(x)$ are the $n \geq 2$ objective functions to be optimized; $h_q(x)$ represents the l equality constraints; and $g_r(x)$ represents the m inequality constraints.

It follows immediately that the global minimizer x^* of the above problem is a Pareto optimal point for the MOP. If this is false, there should be a feasible x, wherein one objective could be improved without sacrificing the others [30].

A common approach is to perform the minimization expressed in Equation 24 repeatedly using an even dispersion of the weight w to generate many points in the Pareto optimal set. However, according to Das and Dennis [30], there are difficulties related to this approach: (1) if the Pareto frontier is nonconvex, there is no weight w for which the solution of the problem remains in the nonconvex area; (2) even with a convex Pareto frontier, a uniform distribution of w does not result in a uniform distribution of the points on the Pareto frontier. Hence, even if a uniform spread of the weight vectors is used, the Pareto frontier will be neither equispaced nor evenly distributed.

According to Shin et al. [31], a multiobjective problem is convex, if both the feasible set Ω and the functions are convex. When at least one objective function is nonconvex, the multiobjective problem becomes nonconvex, generating a nonconvex Pareto frontier that is not connected. When working with the nonconvex Pareto frontiers, the points in the concave area cannot be reached by minimizing the convex combination of the objectives [30]. This instability arises because the weighted sum is not a Lipshitzian function of the weight w [32].

In the RSM, one way to determine the convexity of a function is by characterizing the nature of the stationary point. The stationary point is the level of $x_1, x_2, \ldots, x_k$ that optimizes the predicted response. This point, if it exists, will be the set of $x_1, x_2, \ldots, x_k$, for which the partial derivatives are equal to zero. A general mathematical solution for locating the stationary point may be obtained. The second-order model is expressed in the matrix notation as [21,22]

$$\hat{y} = \hat{\beta}_0 + \mathbf{x}^T\mathbf{b} + \mathbf{x}^T\mathbf{B}\mathbf{x}, \tag{25}$$

where

$$\mathbf{x} = \begin{bmatrix} x_1 \\ x_2 \\ \vdots \\ x_k \end{bmatrix}, \quad \mathbf{b} = \begin{bmatrix} \hat{\beta}_1 \\ \hat{\beta}_2 \\ \vdots \\ \hat{\beta}_k \end{bmatrix},$$

$$\mathbf{B} = \begin{bmatrix} \hat{\beta}_{11} & \hat{\beta}_{12}/2 & \cdots & \hat{\beta}_{1k}/2 \\ \hat{\beta}_{21}/2 & \hat{\beta}_{22} & \cdots & \hat{\beta}_{2k}/2 \\ \vdots & \vdots & \ddots & \vdots \\ \hat{\beta}_{k1}/2 & \hat{\beta}_{k2}/2 & \cdots & \hat{\beta}_{kk} \end{bmatrix} \quad \text{for } \hat{\beta}_{ij} = \hat{\beta}_{ji} \tag{26}$$

The derivative of $\hat{y}$ with respect to the elements of the vector $\mathbf{x}$ equated to zero is

$$\frac{\partial \hat{y}}{\partial \mathbf{x}} = \mathbf{b} + 2\mathbf{B}\mathbf{x} = 0 \tag{27}$$

The stationary point ($\mathbf{x}_s$) is the solution of Equation 27, given by

$$\mathbf{x}_s = -\frac{1}{2}\mathbf{B}^{-1}\mathbf{b} \tag{28}$$

The predicted response ($\hat{y}_s$) at the stationary point is given by

$$\hat{y}_s = \hat{\beta}_0 + \frac{1}{2}\mathbf{x}_s^T\mathbf{b} \tag{29}$$

The nature of the stationary point is determined from the sign of the eigenvalues or characteristic roots of the matrix $\mathbf{B}$. The eigenvalues (λ_i) of the matrix $\mathbf{B}$ are the solutions to the following equation:

$$\left|\mathbf{B} - \lambda\mathbf{I}\right| = 0 \tag{30}$$

where $\mathbf{I}$ is an identity matrix.

If λ_i are all negative, the function is concave, and $\mathbf{x}_S$ is a maximum point; if λ_i are all positive, the function is convex, and $\mathbf{x}_S$ is a minimum point. However, if λ_i have different signs, the function is neither concave nor convex, and $\mathbf{x}_S$ is a saddle point.

3.2. Normal boundary intersection

A standard method for generating the Pareto set in the MOP is the weighted sum method. However, according to Das and Dennis [30], this method can only obtain the points from all parts of the Pareto frontier when it is convex. Furthermore, an evenly distributed set of weights fails to produce an even distribution of the points from all parts of the Pareto frontier, even for convex ones.

To overcome the drawbacks of the weighted sum method, Das and Dennis [33] proposed the NBI method, in which the Pareto surface is evenly distributed and independent of the relative scales and convexities of the objective functions.

Establishing the payoff matrix Φ is the first step of this method. In the matrix notation, Φ can be written as [32,34]

$$\Phi = \begin{bmatrix} f_1^*\left(x_1^*\right) & \cdots & f_1\left(x_i^*\right) & \cdots & f_1\left(x_m^*\right) \\ \vdots & \ddots & & & \vdots \\ f_i\left(x_1^*\right) & \cdots & f_i^*\left(x_i^*\right) & \cdots & f_i\left(x_m^*\right) \\ \vdots & & & \ddots & \vdots \\ f_m\left(x_1^*\right) & \cdots & f_m\left(x_i^*\right) & \cdots & f_m^*\left(x_m^*\right) \end{bmatrix} \tag{31}$$

Each row of Φ consists of the minimum and maximum values of the ith objective function $f_i(x)$. These values can be used to normalize the objective functions, generating the normalized payoff matrix $\bar{\Phi}$. This procedure is used when the objective functions are written in different units. They can be expressed as [32]

$$\bar{f}(x) = \frac{f_i(x) - f_i^U}{f_i^N - f_i^U}, \quad i = 1, \ldots, m \tag{32}$$

where $f_i(x)$ is the individual value of the objectives; f_i^U is the Utopia point; and f_i^N is the Nadir point.

The Utopia point is a specific point, generally present outside the feasible region, corresponding to a region where all the objective functions are at their best possible values simultaneously. It is expressed as $f^U = \left[f_1^*\left(x_1^*\right), \ldots, f_i^*\left(x_i^*\right), \ldots, f_m^*\left(x_m^*\right)\right]^T$. The Nadir point is a point in the design space where all the objectives are simultaneously at their worst values. It is expressed as $f^N = \left[f_1^N, \ldots, f_i^N, \ldots, f_m^N\right]^T$.

The convex hull of individual minimum (CHIM) comprises the convex combinations for each row of Φ. The anchor points that correspond to the solution of a single optimization problem $f_i^*\left(x_i^*\right)$ are connected by the Utopia line [34]. $\bar{\Phi}w_i$ is a point in the CHIM, e is a column vector of ones, and D is the distance between the Utopia line and the Pareto frontier, wherein the intersection point between the normal with $\bar{\Phi}w - D\bar{\Phi}e$ represents the set of points on that normal. The boundary of the feasible region corresponds to the maximization of D. Hence, the NBI method is used to solve the MOP using the following equation [33]:

$$\begin{aligned} &\underset{(x,D)}{Max} \quad D \\ &s.t.: \quad \bar{\Phi}w - D\bar{\Phi}e = \bar{F}(\mathbf{x}) \\ &\qquad \mathbf{x} \in \Omega \end{aligned} \tag{33}$$

where w is the convex weighting; D is the distance between the Utopia line and the Pareto frontier; $\bar{F}(\mathbf{x})$ is the vector containing the individual values of the normalized objectives in each run; e is a column vector of ones; and $\bar{\Phi}$ is the normalized payoff matrix.

This problem can be solved iteratively for different values of w, creating a uniformly distributed Pareto frontier [32,33]. A common choice for w is $w_n = 1 - \sum_{i=1}^{n-1} w_i$ [33–36].

4. Weighting methods applied to multiobjective optimization

When solving a MOP, the goal is to find the efficient solutions. The efficiency is a concept equivalent to the Pareto optimality, noninferiority, and nondominance. However, usually, many efficient solutions (an infinite number) that form the efficient set or the Pareto optimal set exist [25]. According to Mela et al. [37], the process of generating the Pareto optimal alternatives is called the multiobjective optimization.

Mathematically, each Pareto optimal point is an equally acceptable solution to a MOP [25], which is generally desirable for obtaining a point as the final solution. However, because of the multidisciplinary nature of the problems related to the machining processes, which are closely related to several multiple criteria that are incommensurable, determining the best solution to be implemented can be a difficult task. According to Mela et al. [37], the process of choosing a single preferred solution among all the computed alternatives is called multiple criteria decision making.

As it is difficult to determine the degree of importance that should be assigned to each objective function [38], the weights eventually attached to each function are subjectively influenced by the preferences of the analyst. By assigning different weights to the representative objective functions of the process characteristics that are to be optimized, the relative importance of each parameter within the analyzed process is considered. This implies that the weights should be assigned to the functions to indicate their relative importance in order to identify the most important parameters during the optimization process, and hence, the priorities are selected [39].

The priority assigned to the criteria has a vital role in achieving the results and should be applied with caution, as the final result varies significantly depending on the importance attached to each objective [40–42]. This can be a problem because the decision makers are often unsure about the exact weights of the objective functions and utility functions to be used [40]. Eliciting direct preference information from the analyst can be counterproductive in real-world decision-making, as the cognitive effort required is considerable [43].

According to Taboada et al. [40], the Pareto set includes all the rational choices, among which the decision maker must select the final solution by comparing several objectives with each other.

Hence, the search is not for an optimal solution, but for a set of solutions that are optimal in the broadest sense, i.e., they are Pareto optimal. Several techniques that can search the solution space for a set of Pareto optimal solutions exist. The main drawback of these methods is probably the various solutions they generate, from which the decision maker must choose the optimum. Hence, it is necessary to bridge the gap between the unique solutions and the Pareto optimal sets [40].

The weighting issue has been discussed in literature for at least forty years. Zeleny [44,45], when solving a linear multiobjective-optimization problem, aimed to answer the following questions: which is the most preferred solution among the generated, non-dominated, and extreme solutions? Can the set of nondominated solutions be reduced such that they consist of sufficiently fewer points for determining a final decision? To answer these questions, the author coined the phrase "traditional entropy measure" as a parameter to gauge the importance of the functions and define the weights to be used to solve problem.

Recently, Shahhosseini et al. [46], to optimize a packed-bed membrane steam-methane reforming (SMR) tubular reactor for sustainable CH_4 conversion, implemented a multiobjective optimization model based on the optimum H_2/CO ratio for the low-temperature Fischer–Tropsch process by selecting the best optimal value using LINMAP, TOPSIS, Shannon's entropy, and Fuzzy Bellman–Zadeh decision-making methods.

Following a different approach, Rocha et al. [47,48] employed Shannon's [49] entropy index associated with an error measure, the global percentage error (GPE), to determine the most preferred Pareto optimal point in a vertical turning MOP solved by using the NBI method. According to the authors, Shannon's entropy index can provide a more reliable assessment of the relative weights of the objectives in the absence of the preferences of the decision maker, and along with an error measure, it can minimize the error of the preferred Pareto optimal point related to the individual optimal responses. The weighting metric ξ, proposed by Rocha et al. [47,48], is obtained using the equation

$$\begin{aligned} &Max \quad \xi = \frac{Entropy}{GPE} \\ &s.t.: \quad \sum_{i=1}^{n} w_i = 1 \\ &\qquad 0 \le w_i \le 1 \end{aligned} \tag{34}$$

where w_i are the weights assigned to the objectives to be optimized.

The *Entropy* in Eq. (34) is calculated using [49]

$$Entropy = -\sum_{i=1}^{m} w_i \ln w_i \tag{35}$$

The *GPE* in Eq. (34) is calculated using [50]

$$GPE = \sum_{i=1}^{m} \left| \frac{y_i^* - T_i}{T_i} \right| \tag{36}$$

where y_i^* is the value of the Pareto-optimal responses; T_i is the defined target; and m is the number of objectives.

Shannon's entropy index is one of several diversity indices used to measure the diversity in the data. The concepts of diversity employed in many fields of science have the combination of only three properties, i.e., variety, balance, and disparity, each of which is necessary; however, diversity features are insufficient [20,51].

Variety is the number of categories in which the elements of a system are apportioned. Considering that the other parameters are fixed, the greater the variety, the greater the diversity. Balance is a function of the division pattern of the elements through the categories. Considering that the other parameters are fixed, the more uniform the balance, the greater the diversity. Finally, disparity refers to how the elements are different from each other. Considering that the other parameters are fixed, the more disparate the elements, the greater the diversity [20].

According to Stirling [20], Shannon's entropy index, expressed in Eq. (35), only includes the variety and balance dimensions. Hence, the author proposed a formulation that incorporated the variety, balance, and disparity:

$$\Delta = \sum_{ij(i \ne j)} d_{ij}^{\alpha} (w_i w_j)^{\beta} \tag{37}$$

Here, d_{ij} is the disparity between two elements; w are the weights representing the proportion of the elements i and j; and α and β are the terms that quantify the importance degree between the disparity and balance, respectively. In this study, the d_{ij} parameter was obtained as the Euclidean distance between the anchor points, i.e., points that optimize each answer individually. It is calculated as follows:

$$\underset{i \ne j}{d_{ij}} = \sqrt{\left[x^*_{1_{f_i(x)}} - x^*_{1_{f_j(x)}}\right]^2 + \left[x^*_{2_{f_i(x)}} - x^*_{2_{f_j(x)}}\right]^2 + \ldots + \left[x^*_{n_{f_i(x)}} - x^*_{n_{f_j(x)}}\right]^2} \tag{38}$$

where $x_1, x_2 \ldots, x_n$ are the decision variables of the problem; $f_i(x)$ and $f_j(x)$ are the objective functions.

According to Stirling [20], the reference case is the one that considers $\alpha = \beta = 1$; in this case, the equation serves as a Shannon's measure but with an additional feature of capturing the disparity.

5. Experimental design and robust weighting

The dry turning tests for the AISI H13 steel with a chemical composition of 0.40% C, 0.35% Mn, 1.0% Si, 5.25% Cr, 1.00% V, and 1.50% Mo, were performed by Campos [52] using a CNC lathe with a maximum rotational speed of 4500 rpm and a power of 18 kW. The workpieces used in the turning process were made with dimensions Ø 50 mm × 100 mm. They had been previously quenched in a vacuum atmosphere at 1000–1040 °C and then tempered. After the heat treatment, an average hardness of 54 ± 1 HRC was obtained. The ceramic inserts with TiN coating (Al_2O_3 + TiN) and wiper geometry, Ref. GC6050WH (ISO code-CNGA 120408 S01525 WH), were used to machine the AISI H13 hardened steel. The tool holder used in the experiments presented a negative geometry with ISO code DCLNL 2020K12 and entering angle $\chi_r = 95°$.

The *Ra* for the finished turning surfaces was measured using a stylus instrument, adhering to ISO/DIS 4287/1E. In the hard turning process, the cutting tool was subjected to high temperatures and pressures near the nose, resulting in the formation of flank and crater wears. The flank tool wear was evaluated using a toolmaker's microscope with 30× magnification and 1 μm resolution. The admissible flank wear (VB = 0.30 mm) was established according to ISO 3685 standard and measured at the corner radius using scanning electron microscopy (SEM) after each run. Fig. 2 shows the flank and crater wears of the cutting tool.

The *Fc* was measured using a piezoelectric dynamometer. The values were continuously monitored and recorded throughout the test using a charge amplifier with data acquisition capability. The *MRR* was calculated using the ratio of the volume of material removed to the time taken to remove it.

By adopting this experimental condition, the workpieces were machined using a range of parameters, which are given in Table 1. The decision variables were analyzed in a coded way to reduce the

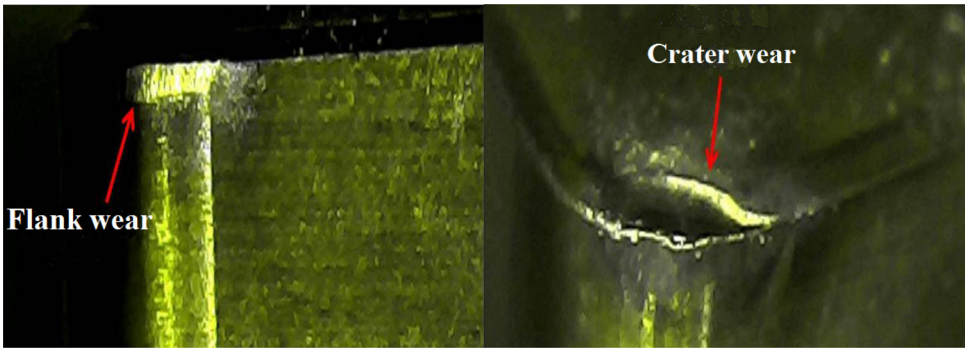

Fig. 2. SEM images of the flank and crater wear of cutting tool.

Source: Campos [52].

Table 1
Parameters used in the experiments.

Factors	Symbol	Levels				
		−1.682	−1	0	1	1.682
Cutting speed (m/min)	*Vc*	57.38	100	162.5	225	267.62
Feed rate (mm/rev)	*f*	0.06	0.10	0.16	0.22	0.26
Depth of cut (mm)	*d*	0.09	0.15	0.24	0.33	0.39

variance. They were decoded only at the end of the analyses. This was done by using the following equation:

$$X_{uncoded} = \frac{Hi + Lo}{2} + X_{coded}\frac{Hi - Lo}{2} \quad (39)$$

where *Hi* is related to the value level +1; *Lo* is related to the value level −1.

A sequential set of experimental runs was established using a CCD built according to the response surface design 2^3, with 6 axial and 5 center points, generating 19 experiments (Table 2).

To optimize the *MRR*, *Ra*, and *Fc* simultaneously, a weighting method was proposed, similar to the multiple criteria decision-making process described by Rocha et al. [48]. It aims to build an evenly distributed Pareto frontier and chooses a preferred Pareto optimal point as the final solution of the problem by maximizing the diversity. In this process, as the NBI method was used, there were no drawbacks related to the weighted sum method. Furthermore, to verify the robustness of the final result obtained with the employed multiobjective optimization process, a metric of the variance was calculated. The aim was to compare the effect of different weighting metrics on the predicted variance. According to Zahran et al. [53], several measures predict the performance of experimental designs, such as the scaled prediction variance (SPV), which is the most commonly used. The SPV is defined as $NVar[\hat{y}(\mathbf{X}_0)]/\sigma^2 = N\mathbf{X}_0^T(\mathbf{X}^T\mathbf{X})^{-1}\mathbf{X}_0$, where N is the total sample size. However, if direct comparisons between the expected variance of the estimation are desired, the unscaled prediction variance (UPV) could be modeled directly by the variance of the estimated mean response divided by σ^2: $Var[\hat{y}(\mathbf{X}_0)]/\sigma^2 = \mathbf{X}_0^T(\mathbf{X}^T\mathbf{X})^{-1}\mathbf{X}_0$. It is equivalent to the Hat Matrix [22].

Fig. 3 shows the step-by-step proposal.

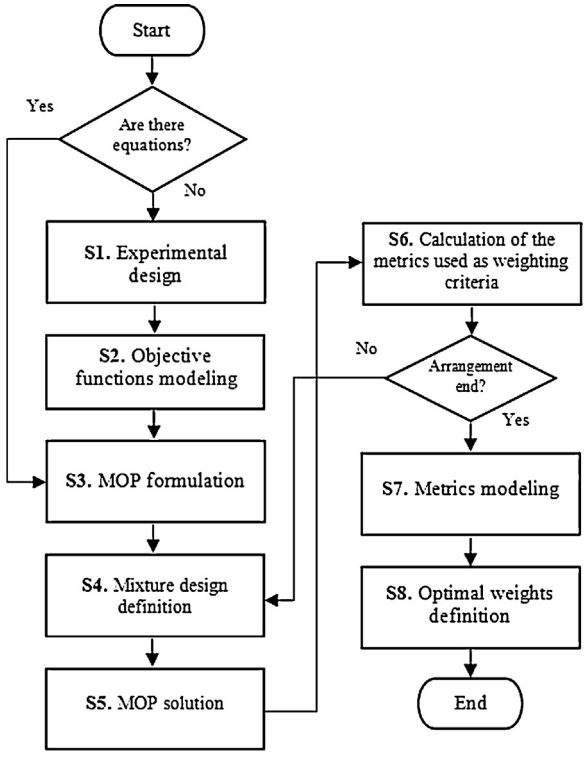

Fig. 3. Step-by-step proposal.
Source: Adapted from Rocha et al. [54].

6. Results and discussion

An analysis of experimental data generated the mathematical models for *MRR* (cm^3/min), *Ra* (μm), and *Fc* (N) presented in Eqs. (40)–(42), respectively. An ANOVA showed that the models were adequate, as the *p*-values of the analyzed objective functions had a statistically significant regression at a 5% level of significance. Moreover, the adjusted R^2 values of 99.24%, 92.24%, and 95.45% for *MRR* (cm^3/min), *Ra* (μm), and *Fc* (N), respectively, showed that the models had a good adjustment. Although the *Ra* had the worst adjusted R^2, 92.24%, it was still considered acceptable [21,22].

In Eqs. (40)–(42), the values in bold represent significant terms in the model:

$$MRR\,(\mathrm{cm}^3/\mathrm{min}) = \mathbf{6.340} + \mathbf{2.438}\boldsymbol{Vc} + \mathbf{2.438}\boldsymbol{f} + \mathbf{2.377}\boldsymbol{d} - 0.001d^2 + \mathbf{0.935}(\boldsymbol{Vc}\times\boldsymbol{f}) + \mathbf{0.915}(\boldsymbol{Vc}\times\boldsymbol{d}) + \mathbf{0.915}(\boldsymbol{f}\times\boldsymbol{d}) \quad (40)$$

Table 2
CCD for *MRR*, *Ra*, and *Fc*.

No.	*Vc* (m/min)	*f* (mm/rev)	*d* (mm)	*MRR* (cm^3/min)	*Ra* (μm)	*Fc* (N)
1	−1	−1	−1	1.5	0.13	340.221
2	+1	−1	−1	3.38	0.11	236.493
3	−1	+1	−1	3.38	0.41	432.593
4	+1	+1	−1	7.59	0.72	240.32
5	−1	−1	+1	3.3	0.34	451.47
6	+1	−1	+1	7.43	0.09	244.18
7	−1	+1	+1	7.43	0.08	459.395
8	+1	+1	+1	16.71	0.42	246.31
9	−1.682	0	0	2.24	0.22	485.87
10	+1.682	0	0	10.44	0.29	224.48
11	0	−1.682	0	2.24	0.13	319.28
12	0	+1.682	0	10.44	0.49	358.85
13	0	0	−1.628	2.34	0.22	330.98
14	0	0	+1.682	10.33	0.12	359.24
15	0	0	0	6.34	0.47	336.52
16	0	0	0	6.34	0.49	335.28
17	0	0	0	6.34	0.49	334.92
18	0	0	0	6.34	0.48	337.83
19	0	0	0	6.34	0.47	334.78

Source: Adopted from Campos [52].

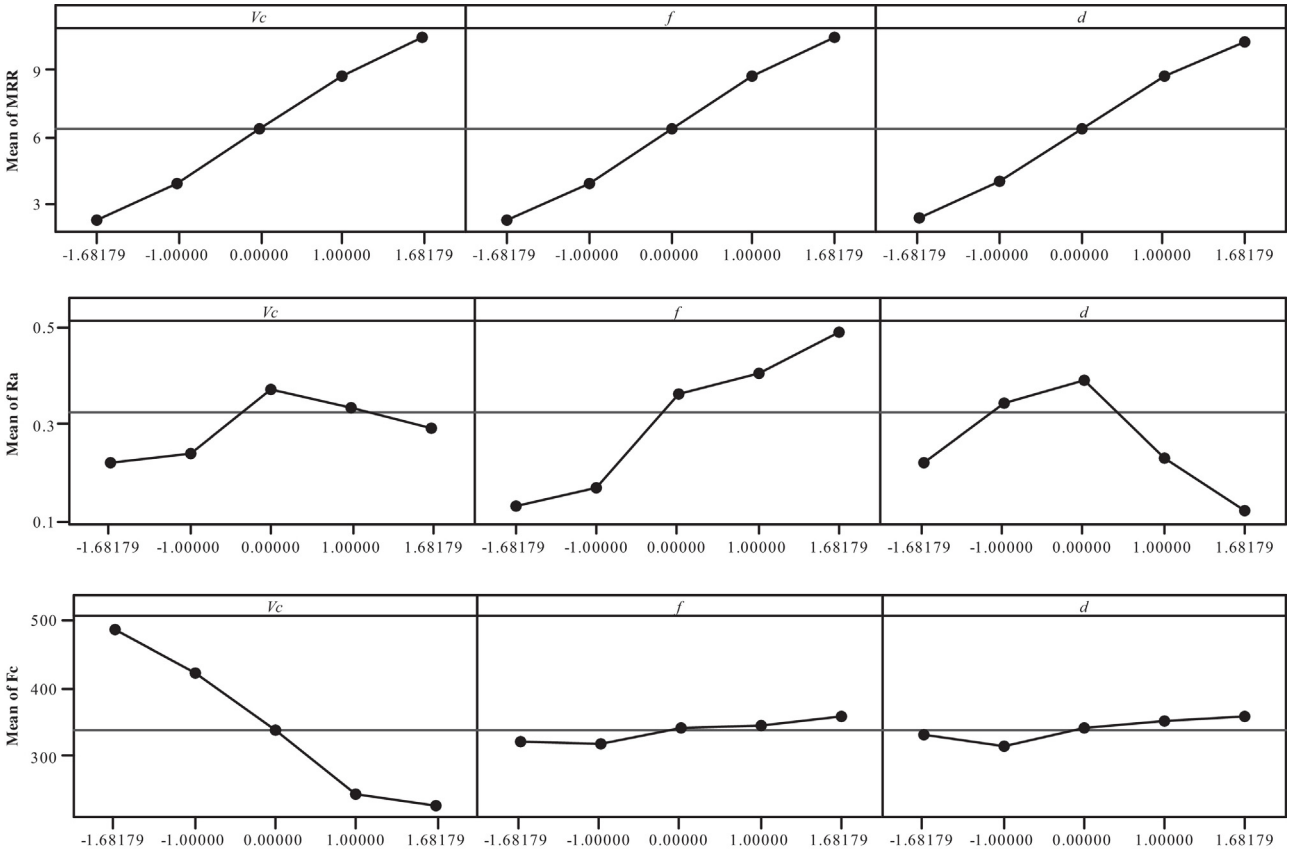

Fig. 4. Main effect plots for *MRR*, *Ra* and *Fc*.

For *MRR*, the model draws attention the statistical significance of the interaction terms $Vc \times f$, $Vc \times d$, and $f \times d$. It proves that a synergistic effect exists between *Vc*, *f*, and *d* in the productivity parameter *MRR*:

$$Ra(\mu m) = \mathbf{0.478} + \mathbf{0.036}Vc + \mathbf{0.115}f - \mathbf{0.045}d - \mathbf{0.067}Vc^2 - \mathbf{0.048}f^2 - \mathbf{0.098}d^2 + \mathbf{0.115}(Vc \times f) - 0.025(Vc \times d) - \mathbf{0.103}(f \times d) \quad (41)$$

For *Ra*, the interaction terms $Vc \times f$ and $f \times d$ are significant. While $f \times d$ improves the *Ra* values, the interaction between *Vc* and *f* impairs the *Ra* values, damaging the quality of the machined part:

$$Fc(N) = \mathbf{336.475} - \mathbf{84.645}Vc + \mathbf{12.653}f - \mathbf{14.590}d + 3.475Vc^2 - 2.221f^2 - 0.083d^2 - 11.793(Vc \times f) - \mathbf{15.547}(Vc \times d) - 10.768(f \times d) \quad (42)$$

For *Fc*, the interaction term $Vc \times d$ contributes to decreasing the *Fc* values, which is desirable in that process.

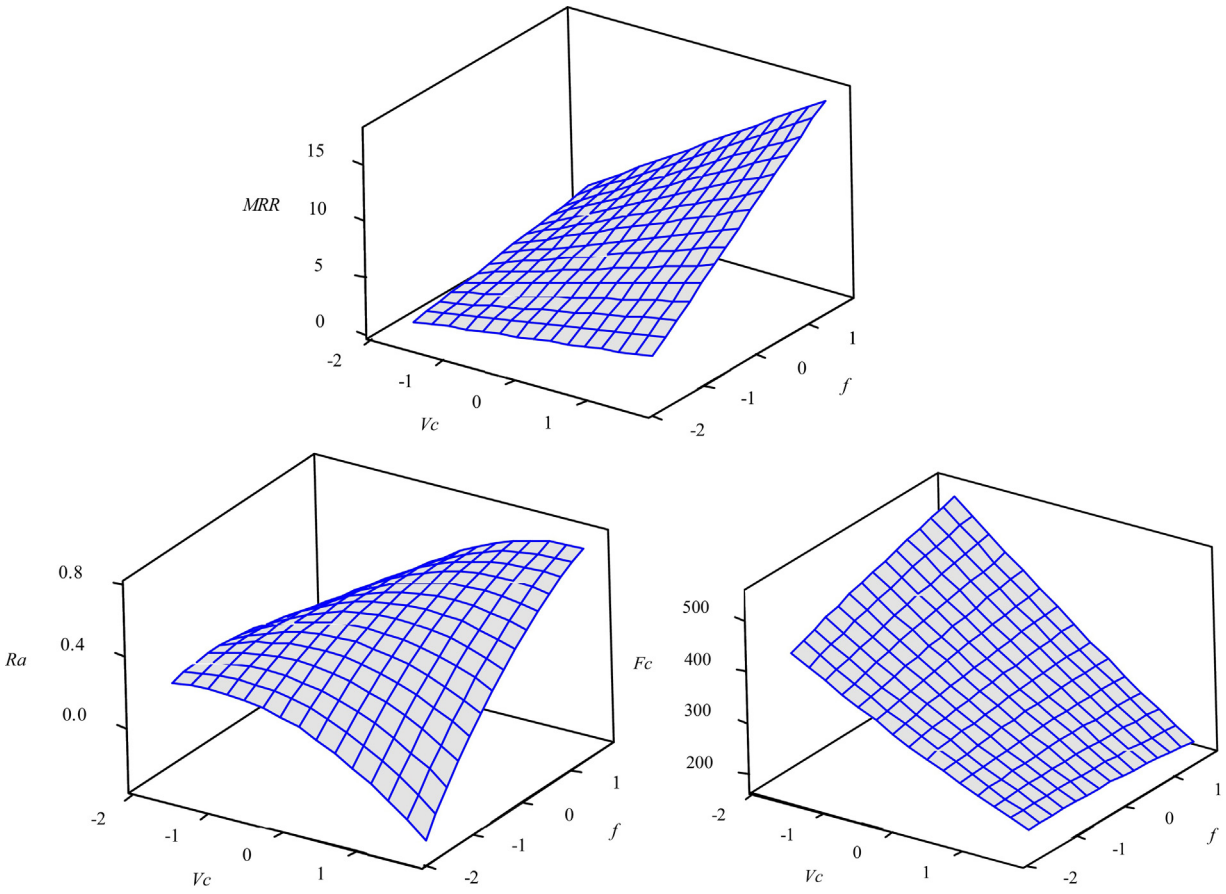

Fig. 5. Response surface for *MRR*, *Ra* and *Fc* (hold value: $d = 0$).

In order to compare how each decision variable affected each response, the main effect plots for *MRR*, *Ra*, and *Fc* were plotted; they are shown in Fig. 4.

The figures showed that *Vc*, *f*, and *d* were equally significant in increasing *MRR*, which is justified by the fact that these variables directly affect the productivity of the process. The factor *f* was more significant than other factors in increasing *Ra*, which agreed with the results obtained by Özel et al. [11], who analyzed a CBN tool with wiper geometry in AISI H13 hardened steel turning. The behavior of the responses of *MRR* and *Ra* that were related to the variation in *f* highlighted the conflicting nature of the objective functions. If the goal is to increase productivity, an increase in *f* can drastically increase the *Ra*, damaging the quality. *Vc* increased *Ra* until a value of 0.000 (162.5 m/min), but beyond this value, it decreased *Ra*. This result is different from that described by Ferreira et al. [16], who found evidence that higher values of *Vc* increase *Ra*. The factor *d* had the same effect on *Ra* as *Vc*, since it increased *Ra* until a value of 0.000 (0.24 mm), decreasing *Ra* beyond this value. For *Fc*, compared with other factors, *Vc* had the most significant effect on decreasing *Fc*, similar to the results obtained by Özel et al. [11].

Fig. 5 shows the response surfaces for *MRR*, *Ra*, and *Fc*.

Fig. 5 confirms the conflicting nature of the objectives. While an increase in *f* caused an increase in *MRR*, it also caused an increase in *Ra*, which is undesirable from a quality point of view. Furthermore, *Fc* had a conflicting relationship with *Ra*, since a reduction in *Fc* was associated with an increase in *Ra*. On the other hand, *MRR* and *Fc* had less conflicting relationship, since a decrease in *Fc* increased *MRR*, which is desirable in the analyzed process. In order to check the convexities of the functions, before performing the multiobjective optimization, the natures of the stationary points were analyzed by using Eq. (30). For *MRR*, the eigenvalues (λ_i) were [0.9215; −0.4671; −0.4550], i.e., the different eigenvalues signs indicated that the function was neither concave nor convex, and the stationary point was a saddle point. For *Ra* and *Fc*, the eigenvalues (λ_i) were [−0.1384; −0.0948; 0.0202] and [−12.4186; 9.8617; 3.7278], respectively, and in both the cases the stationary points were saddle points. An analysis of the natures of the stationary points revealed that the functions had different convexities and, therefore, the weighted sum method for multiobjective optimization was not the most suitable approach, according to Das and Dennis [30]. Thus, in this work the NBI method was used. To implement the NBI optimization routine, the payoff matrix was first estimated; the obtained results are reported in Table 3.

Table 3
Payoff matrix for the objective functions.

MRR	Ra	Fc
15.988	0.373	245.406
2.433	**0.014**	258.586
12.343	0.382	**201.408**

Bold values represent individual optimums.

The results in Table 3 were obtained by the individual optimization of the mathematical models of *MRR*, *Ra*, and *Fc*. It is possible to see that, in the *MRR* maximum response, *Ra* and *Fc* values are jeopardized. Moreover, when minimizing *Fc*, the *Ra* value is the most negatively affected.

Once the NBI was implemented, a mixture design for the weights of each objective function was defined. Subsequently, the solution of the optimization problem of NBI was obtained for each experimental condition defined by the mixture design. Based on these results, the weighting metric ξ, diversity, and UPV were calculated.

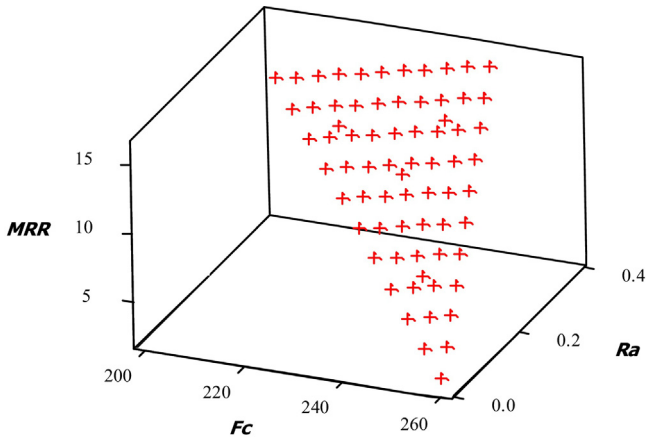

Fig. 6. Pareto frontier for *MRR Ra* and *Fc*.

Table 4
Pearson correlation.

	Diversity	ξ
ξ	0.626 0.000	
UPV	−0.795 0.000	−0.199 0.098

The results presented in Fig. 6 comprise the Pareto optimal set for the multiobjective problem. By changing the weights or the degrees of importance assigned to each response, the results of the optimization process could be altered, favoring the response with the highest weight. The utilization of MDE along with the NBI method makes it easier to define a Pareto frontier with evenly distributed solutions, regardless of the convexity of the functions. Once again, the conflicting nature of the responses is evident, as *Ra* and *Fc* are negatively affected when *MRR* is maximized.

As one of the objectives of RSM is to optimize the responses, it is recommended, whenever possible, to represent the responses by second-order models, as their curvatures define the location of stationary points. In the case of first-order designs, the dominant property is orthogonality. In the case of second-order designs, the orthogonality is no longer an important aspect, and the estimation of the individual coefficients, once considered important, becomes secondary. The UPV becomes the property of greater importance. This stems from the fact that the quality of $\hat{y}(x)$ as a predictor or estimator of $E[y(x)]$ is more important than the variables in the model. Thus, lower values of UPV provide assurance of the quality of $\hat{y}(x)$ as a predictor of the future values of the responses, since the analyst does not know from the beginning where in the experimental space it will necessarily be to make predictions or where the optimum will be.

Regarding the values of UPV, it is important to note they changed with changes in the results of the optimization process, i.e., the prediction variance behavior was related to the weighting. This result confirms that the robustness of the optimization process is associated with the choice of the Pareto optimal point as the final solution for the MOP. Table 4 presents a Pearson correlation analysis between the values of the metrics calculated for each point presented in Fig. 6. *p*-Values less than 5% indicate statistically significant correlations.

The Pearson correlation analysis showed that the diversity index had a negative and statistically significant correlation with UPV, i.e., by maximizing this metric, the variance values tended to be lower. This information provides us with evidence that the search for the most preferred Pareto optimal point in multiobjective optimization using this metric leads to a robust response from the variability point of view. The weighting metric ξ has a less negative and statistically significant correlation with UPV when compared with the diversity index (Figs. 7–9).

Table 5
Confidence intervals.

Responses	Lower limit	Mean	Upper limit
MRR	8.8487	9.3330	9.8173
Ra	0.1343	0.2098	0.2853
Fc	221.6442	245.8975	270.1508

Following the Pearson correlation analysis, the modeling of the weighting metric ξ, diversity, and UPV was done. Their canonical polynomials of mixture, response surfaces, and contour plots were:

$$\begin{aligned}\xi = {} & -0.0025w_1 + 0.0202w_2 - 0.0023w_3 + 0.1525w_1w_2 + 0.1216w_1w_3 \\ & + 0.1542w_2w_3 - 0.2207w_1w_2(w_1 - w_2) + 0.1972w_2w_3(w_2 - w_3) \\ & + 0.4867w_1w_1w_2w_3 + 0.3633w_1w_2(w_1 - w_2)^2 + 0.3565w_2w_3(w_2 - w_3)^2\end{aligned} \tag{43}$$

$$Diversity = 2.9314w_1w_2 + 1.2205w_1w_3 + 2.1535w_2w_3 \tag{44}$$

$$\begin{aligned}UPV = {} & 0.6056w_1 + 0.6128w_2 + 0.6057w_3 - 0.6731w_1w_2 \\ & -0.4952w_1w_3 - 0.6835w_2w_3 \\ & - 0.8665w_1w_2(w_1 - w_2) + 0.0271w_2w_3(w_2 - w_3) \\ & +0.6539w_1w_1w_2w_3 \\ & - 0.9403w_1w_2w_2w_3 - 0.5356w_1w_2w_3w_3 \\ & -0.2263w_1w_2(w_1 - w_2)^2 \\ & - 0.1017w_1w_3(w_1 - w_3)^2 - 0.1084w_2w_3(w_2 - w_3)^2\end{aligned} \tag{45}$$

It should be noted that all the canonical polynomials of mixture had good fitness, since almost all have adjusted R^2 values close to 100%. The weighting metric ξ had the worst adjusted R^2, 94.82%. Even so, this value was considered acceptable [21,22]. It is worth noting that it was possible to model the metrics of variance and UPV in terms of their weights. This is because the weights interfere in the solution space. However, since optimizations of distinct functions are performed simultaneously, the solution space is not the same initial area of the DOE, and therefore, when modeling the variance, its shape is distinguishable from the Hat Matrix shape.

Lastly, by the maximization of diversity, described in Equation 44, the weights w_1, w_2, and w_3, related to the final solution were found. The values were as follows: $w_1 = 0.4171$; $w_2 = 0.4571$; and $w_3 = 0.1258$. These optimal weights were used in a multiobjective optimization of *MRR*, *Ra*, and *Fc*, generating values of 9.3330 cm^3/min, 0.2098 μm, and 245.8975 N, respectively. This result was considered acceptable when compared with the results of other hardened steels reported in literature [2,7,8,12,55–62]. The optimal coded values of the decision variables were as follows: $Vc = 1.1462$, $f = -0.5657$, and $d = 0.7511$. The coded values were transformed into uncoded values by the use of Eq. (39). Thus, the optimal values of the decision variables were as follows: $Vc = 234.1399$ m/min, $f = 0.1261$ mm/rev, and $d = 0.3076$ mm.

Fig. 10 shows the Pareto frontier built using the NBI method, with the optimal highlighted.

In Fig. 10, it was shown that the Pareto optimal points on the frontier were evenly distributed. Moreover, we could find the most preferred Pareto optimal point in Fig. 10 as the final solution for the MOP. Table 5 shows the confidence intervals for the responses associated with the optimal point. Eq. (15) is used, and the adopted probability is 95%, i.e., $\alpha = 5\%$.

From the variability point of view, the final solution obtained with the maximization of diversity was robust, since this metric led the solution to a region of minimum variance, less variability,

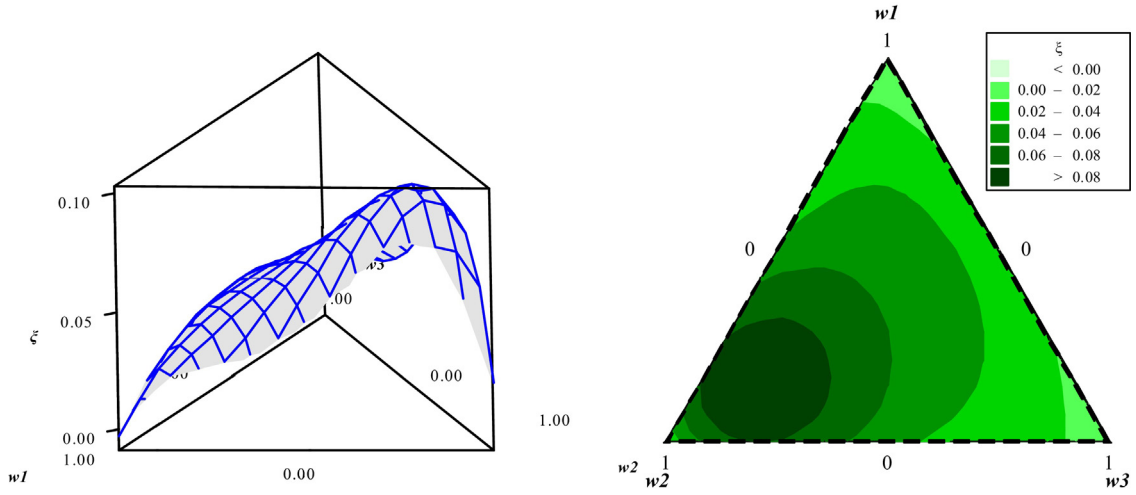

Fig. 7. ξ response surface and contour plot.

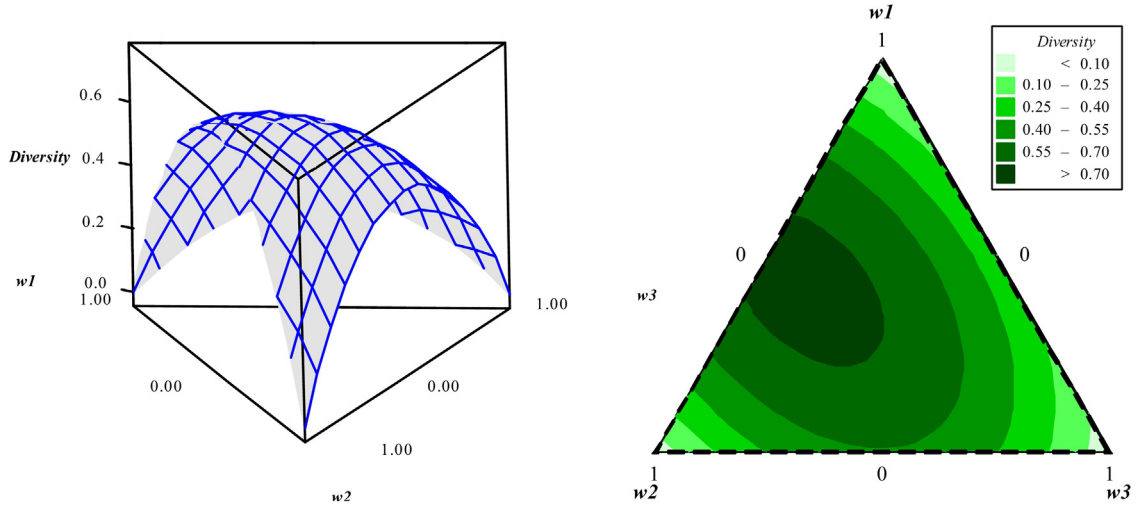

Fig. 8. Diversity response surface and contour plot.

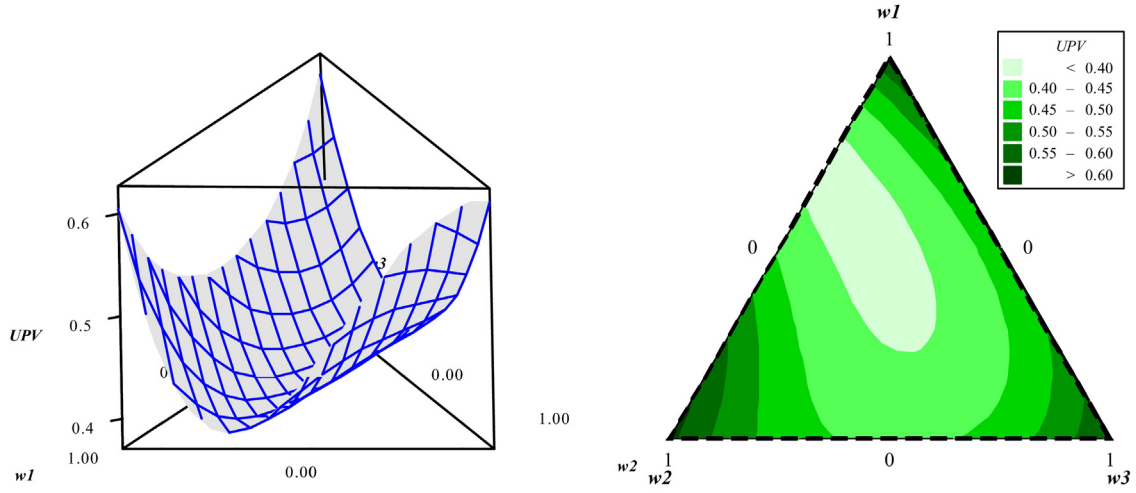

Fig. 9. UPV response surface and contour plot.

and greater reliability. However, the confidence interval of *Ra* was higher than those of the other responses. It proves that *Ra* is the most difficult parameter to control in the analyzed process.

Fig. 11 shows the overlap of the different objective functions defining the feasible region for the problem. Fig. 11 shows the conflicting nature between *MRR* and the other responses, i.e., an

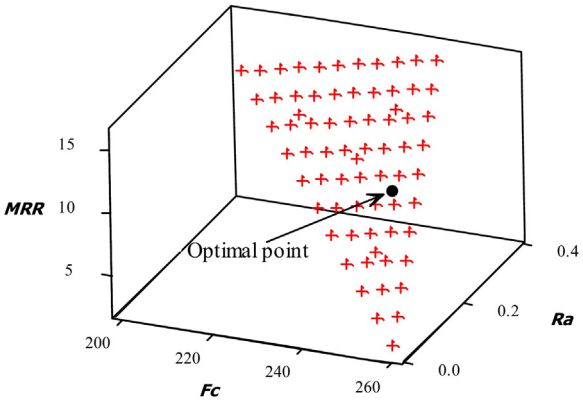

Fig. 10. Optimal point identification in the Pareto frontier.

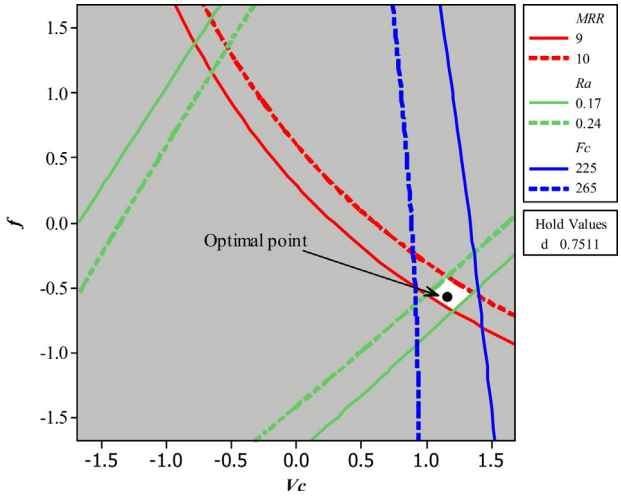

Fig. 11. Point of optimization for *MRR*, *Ra*, and *Fc*.

increase in *MRR* leads to an increase in *Ra* and *Fc*. In this work, the optimal point was chosen based on the maximization of diversity, and it was proved that this point was robust, since its UPV value was the lowest found within the solution region delimited by the MOP. This finding demonstrates the importance of the proposed method, which provides robust responses with lower prediction variance and without complex calculations. In addition, the proposed method is considered relevant, since the topic of robust optimization remains highlighted in the literature [7,56,57,63,64].

7. Conclusions

A novel robust optimization process combining the NBI method and the diversity approach was successfully employed to optimize the turning process of AISI H13 hardened steel with a ceramic wiper tool. The NBI method was used to optimize the *MRR*, *Ra*, and *Fc* simultaneously, helping to build an evenly distributed Pareto frontier for the three responses, regardless of the convexity of the functions. As a result, the diversity-based weighting was able to generate a combination of weights that led to the minimization of the prediction variance of the analyzed responses. This decision-making criterion proved to be useful for mapping the regions of minimum variance within the Pareto optimal responses obtained in the optimization process, i.e., the study proves the robustness of the weighting process employed to choose the final solution.

The Stirling diversity index [20,51] was used to select the most preferred Pareto optimal point as the final solution. Although some studies make use of this index for the diversification of the energetic matrix, among the studies reviewed, none used this metric for the multiobjective optimization processes.

It was possible to model the metric of variance, UPV, in terms of weights, because the weights influenced the solution space. Hence, the study demonstrated that the weights used in the multiobjective optimization process influenced the prediction variance of the obtained responses. As many studies resort to multiobjective optimization and have as one of their objectives to reduce the prediction variance of the estimated response, this is the main contribution of this work to studies in the area.

We noticed that the benefits of this weighting based on diversity were considerably more useful for estimated models, such as surface models, as they reduced the forecast error, considering that the prediction variance is a subject of major importance when working with second-order response surface models. As many studies in the field use RSM, once again the contribution of this proposed method is demonstrated.

The responses' mathematical models presented an acceptable fitting, proving the adequacy of the functions. The following were the main results of this study: a synergistic effect was observed between the *Vc*, *f*, and *d* in the productivity parameter *MRR*; a synergistic effect was observed between *f* and *d* in improving the *Ra* values; and a synergistic effect was observed between *Vc* and *d* in decreasing *Fc* values. The factors *Vc*, *f*, and *d* were equally significant in increasing the *MRR*. The variable *f* was identified as the most significant factor for increasing *Ra*, which is undesirable. The variable *Vc* was identified as the most significant factor for decreasing *Fc*.

The simultaneous optimal values for the objective functions *MRR*, *Ra*, and *Fc* were 9.3330 cm^3/min, 0.2098 μm, and 245.8975 N, respectively These results were obtained by using the following combination of the process parameters: *Vc* = 234.1399 m/min, *f* = 0.1261 mm/rev, and *d* = 0.3076 mm. The analyses of the confidence interval of the responses showed that *Ra* has greater variability, as it was the most difficult parameter to control in the analyzed process.

Conflicts of interest

The authors would like to declare that they have no conflicts of interests.

Acknowledgments

The authors would like to thank the Brazilian Government agencies CNPq, CAPES, FAPEMIG, and IFSULDEMINAS for their support. The authors would also like to acknowledge the University of Aveiro for their fundamental contribution to this study.

References

[1] Özel T, Karpat Y, Figueira L, Davim JP. Modelling of surface finish and tool flank wear in turning of AISI D2 steel with ceramic wiper inserts. J Mater Process Technol 2007;189(1–3):192–8.
[2] Bouacha K, Yallese MA, Mabrouki T, Rigal JF. Statistical analysis of surface roughness and cutting forces using response surface methodology in hard turning of AISI 52100 bearing steel with CBN tool. Int J Refract Met Hard Mater 2010;28(3):349–61.
[3] Çiçek A, Kara F, Kivak T, Ekici E. Evaluation of machinability of hardened and cryo-treated AISI H13 hot work tool steel with ceramics inserts. Int J Refract Met Hard Mater 2013;41:461–9.
[4] Chinchanikar S, Choudhury SK. Machining of hardened steel-experimental investigations, performance modeling and cooling technique: a review. Int J Mach Tools Manuf 2015;89:95–109.
[5] Yallese MA, Bouacha K, Rigal JF, Mabrouki T. Statistical analysis of surface roughness and cutting forces using response surface methodology in hard turning of AISI 52100 bearing steel with CBN tool. Int J Refract Met Hard Mater 2010;28:349–61.
[6] Bouacha K, Yallese MA, Khamel S, Belhadi S. Analysis and optimization of hard turning operation using cubic boron nitride tool. Int J Refract Met Hard Mater 2014;45:160–78.

[7] Paiva AP, Campos PH, Ferreira JR, Lopes LGD, Paiva EJ, Balestrassi PP. A multivariate robust parameter design approach for optimization of AISI 52100 hardened steel turning with wiper mixed ceramic tool. Int J Refract Met Hard Mater 2012;30:152–63.
[8] Grzesik W. Wear development on wiper Al_2O_3–TiC mixed ceramic tools in hard machining of high strength steel. Wear 2009;266(9–10):1021–8.
[9] Grzesik W. Influence of tool wear on surface roughness in hard turning using differently shaped ceramic tools. Wear 2008;265(3–4):327–35.
[10] Wang B, Liu Z. Cutting performance of solid ceramic end milling tools in machining hardened AISI H13 steel. Int J Refract Met Hard Mater 2016;55:24–32.
[11] Özel T, Hsu TK, Zeren E. Effects of cutting edge geometry, workpiece hardness, feed rate and cutting speed on surface roughness and forces in finish turning of hardened AISI H13 steel. Int J Adv Manuf Technol 2005;25(3):262–9.
[12] Gaitonde VN, Karnik SR, Figueira L, Davim JP. Machinability investigations in hard turning of AISI D2 cold work tool steel with conventional and wiper ceramic inserts. Int J Refract Met Hard Mater 2009;27(4):754–63.
[13] Diniz A, Ferrer J. A comparison between silicon nitride-based ceramic and coated carbide tools in the face milling of irregular surfaces. J Mater Process Technol 2008;206(1–3):294–304.
[14] Long Y, Zeng J, Shanghua W. Cutting performance and wear mechanism of Ti–Al–N/Al–Cr–O coated silicon nitride ceramic cutting inserts. Ceram Int 2014;40(7):9615–20.
[15] Oh S, Ahn S, Oh K, Lee H, Chung T. Investigation into the microstructure and cutting performance of (Ti,Ta, W)(CN)–Co/Ni cements. Int J Refract Met Hard Mater 2015;53:36–40.
[16] Ferreira R, Řehoř J, Lauro CH, Carou D, Davim JP. Analysis of the hard turning of AISI H13 steel with ceramic tools based on tool geometry: surface roughness, tool wear and their relation. J Braz Soc Mech Sci Eng 2016, http://dx.doi.org/10.1007/s40430-016-0504-z (in press).
[17] Correia AE, Davim JP. Surface roughness measurement in turning carbon steel AISI 1045 using wiper inserts. Measurement 2011;44(5):1000–5.
[18] Elbah M, Yallese M, Aouici H, Mabrouki T, Rigal J. Comparative assessment of wiper and conventional ceramic tools on surface roughness in hard turning AISI 4140 steel. Measurement 2013;46(9):3041–56.
[19] Anderson-Cook CM, Borror CM, Montgomery DC. Response surface design evaluation and comparison. J Stat Plan Inference 2009;139(2):629–41.
[20] Stirling A. A general framework for analysing diversity in science, technology and society. J R Soc Interface 2007;4(15):707–19.
[21] Montgomery DC. Design and analysis of experiments. 5th ed. New York: John Wiley & Sons; 2001.
[22] Myers RH, Montgomery DC, Anderson-Cook CM. Response surface methodology: process and product optimization using designed experiments. 3rd ed. New York: John Wiley & Sons; 2009, 680 pp.
[23] Box GEP, Draper NR. Empirical model-building and response surfaces. New York: John Wiley & Sons; 1987.
[24] Cornell J. Experiments with mixtures: designs, models, and the analysis of mixture data. 3rd ed New York: John Wiley & Sons; 2002.
[25] Miettinen K. Nonlinear multiobjective optimization. Boston: Kluwer Academic Publishers; 1999.
[26] Baril C, Yacout S, Clément B. Design for Six Sigma through collaborative multiobjective optimization. Comput Ind Eng 2011;60(1):43–55.
[27] Shahraki AF, Noorossana R. Reliability-based robust design optimization: a general methodology using genetic algorithm. Comput Ind Eng 2014;74:199–207.
[28] Hwang CL, Masud ASM. Multiple objective decision making—methods and applications: a state-of-the-art survey, vol. 164 of Lecture notes in economics and mathematical systems. Berlin/New York: Springer; 1979.
[29] Zhang W, Yang H. A study of the weighting method for a certain type of multicriteria optimization problem. Comput Struct 2001;79(31):2741–9.
[30] Das I, Dennis JE. A closer look at drawbacks of minimizing weighted sums of objectives for Pareto set generation in multicriteria optimization problems. Struct Optim 1997;14(1):63–9.
[31] Shin S, Samanlioglu F, Cho BR, Wiecek MM. Computing trade-offs in robust design: perspectives of the mean squared error. Comput Ind Eng 2011;60(2):248–55.
[32] Vahidinasab V, Jadid S. Normal boundary intersection method for suppliers' strategic bidding in electricity markets: an environmental/economic approach. Energy Convers Manage 2010;51(6):1111–9.
[33] Das I, Dennis JE. Normal boundary intersection: a new method for generating the Pareto surface in nonlinear multicriteria optimization problems. SIAM J Optim 1998;8(3):631–57.
[34] Utyuzhnikov SV, Fantini P, Guenov MD. A method for generating a well-distributed Pareto set in nonlinear multiobjective optimization. J Comput Appl Math 2009;223(2):820–41.
[35] Shukla PK, Deb K. On finding multiple Pareto-optimal solutions using classical and evolutionary generating methods. Eur J Oper Res 2007;181(3):1630–52.
[36] Jia Z, Ierapetritou G. Generate Pareto optimal solutions of scheduling problems using normal boundary intersection technique. Comput Chem Eng 2007;31(4):268–80.
[37] Mela K, Tiainen T, Heinisuo M, Baptiste P. Comparative study of multiple criteria decision making methods for building design. Adv Eng Inform 2012;26:716–26.
[38] Szeląg M, Greco S, Słowiński R. Variable consistency dominance-based rough set approach to preference learning in multicriteria ranking. Inform Sci 2014;277(1):525–52.
[39] Ibáñes-Forés V, Bovea MD, Pérez-Belis V. A holistic review of applied methodologies for assessing and selecting the optimal technological alternative from a sustainability perspective. J Cleaner Prod 2014;70(1):259–81.
[40] Taboada HA, Baheranwala F, Coit DW, Wattanapongsakorn N. Practical solutions for multi-objective optimization: an application to system reliability design problems. Reliab Eng Syst Saf 2007;92(3):314–22.
[41] Gaudreault C, Samson R, Stuart P. Implications of choices and interpretation in LCA for multi-criteria process design: de-inked pulp capacity and cogeneration at a paper mill case study. J Cleaner Prod 2009;17(17):1535–46.
[42] Pilavachi PA, Stephanidis SD, Pappas VA, Afgan NH. Multi-criteria evaluation of hydrogen and natural gas fuelled power plant technologies. Appl Therm Eng 2009;29(11–12):2228–34.
[43] Figueira JR, Greco S, Słowiński R. Building a set of additive value functions representing a reference preorder and intensities of preference: GRIP method. Eur J Oper Res 2009;195(2):460–86.
[44] Zeleny M. A concept of compromise solutions and the method of the displaced ideal. Comput Oper Res 1974;1(3–4):479–96.
[45] Zeleny M. The theory of the displaced ideal. In: Zeleny M, editor. Lecture notes in economics and mathematical systems, no. 123: multiple criteria decision making – Kyoto. Berlin/New York: Springer-Verlag; 1975.
[46] Shahhosseini HR, Farsi M, Eini S. Multi-objective optimization of industrial membrane SMR to produce syngas for Fischer–Tropsch production using NSGA-II and decision makings. J Nat Gas Sci Eng 2016;32:222–38.
[47] Rocha LCS, Paiva AP, Balestrassi PP, Severino G, Rotela Junior P. Entropy-based weighting for multiobjective optimization: an application on vertical turning. Math Probl Eng 2015. Article ID 608325.
[48] Rocha LCS, Paiva AP, Balestrassi PP, Severino G, Rotela Junior P. Entropy-based weighting applied to normal boundary intersection approach: the vertical turning of martensitic gray cast iron piston rings case. Acta Sci Technol 2015;37(4):361–71.
[49] Shannon CE. A mathematical theory of communication. Bell Syst Techn J 1948;27:379–423, 623–56.
[50] Rocha LCS, Paiva AP, Paiva EJ, Balestrassi PP. Comparing DEA and principal component analysis in the multiobjective optimization of P-GMAW process. J Braz Soc Mech Sci 2015, http://dx.doi.org/10.1007/s40430-015-0355-z (in press).
[51] Stirling A. Diversity and ignorance in electricity supply investment: addressing the solution rather than the problem. Energy Policy 1994;22(3):195–216.
[52] Campos PHS (Doctoral dissertation) Metodologia DEA-OTS: Uma contribuição para a seleção ótima de ferramentas no Torneamento do Aço ABNT H13 Endurecido. Brazil: Universidade Federal de Itajubá; 2015.
[53] Zahran A, Anderson-Cook CM, Myers RH. Fraction of design space to assess prediction capability of response surface designs. J Qual Technol 2003;35(4):377–86.
[54] Rocha LCS, Paiva AP, Rotela Junior P, Balestrassi PP, Campos PH. Robust multiple criteria decision making applied to optimization of AISI H13 hardened steel turning with PCBN wiper tool. Int J Adv Manuf Technol 2015, http://dx.doi.org/10.1007/s00170-016-9250-8 (in press).
[55] Mandal N, Doloi B, Mondal B. Development of flank wear prediction model of zirconia toughened alumina (ZTA) cutting tool using response surface methodology. Int J Refract Met Hard Mater 2011;29(2):273–80.
[56] Paiva AP, Ferreira JR, Balestrassi PP. A multivariate hybrid approach applied to AISI 52100 hardened steel turning optimization. J Mater Process Technol 2007;189(1–3):26–35.
[57] Paiva AP, Paiva EJ, Ferreira JF, Balestrassi PP, Costa SC. A multivariate mean square error optimization of AISI 52100 hardened steel turning. Int J Adv Manuf Technol 2009;43(7):631–43.
[58] Huang Y, Chou YK, Liang SY. CBN tool wear in hard turning: survey on research progresses. Int J Adv Manuf Technol 2007;35(5):443–53.
[59] Tamizharasan T, Sevaraj T, Haq AN. Analysis of tool wear and surface finish in hard turning. Int J Adv Manuf Technol 2006;28(7):671–9.
[60] Singh D, Rao PV. A surface roughness model for hard turning process. Int J Adv Manuf Technol 2007;32(11):1115–24.
[61] Diniz AE, Ferreira JR, Filho FT. Influence of refrigeration/lubrication condition on SAE 52100 hardened steel turning at several cutting speeds. Int J Mach Tools Manuf 2003;42(3):317–26.
[62] Lima JG, Ávila RF, Abrão AM, Faustino M, Davim JP. Hard turning: AISI 4340 high strength low alloy steel and AISI D2 cold work tool steel. J Mater Process Technol 2005;169(3):388–95.
[63] Brito TG, Paiva AP, Ferreira JR, Gomes JHF, Balestrassi PP. A normal boundary intersection approach to multiresponse robust optimization of the surface roughness in end milling process with combined arrays. Precis Eng 2014;38:628–38.
[64] Gomes JHF, Paiva AP, Costa SC, Balestrassi PP, Paiva EJ. Weighted multivariate mean square error for processes optimization: a case study on fluxcored arc welding for stainless steel claddings. Eur J Oper Res 2013;226:522–35.